IEEE Photonics Journal
An IEEE Photonics Society Publication

Open Access

All-Fiber Light Intensity Detector Based on an Ionic-Liquid-Adorned Microstructured Optical Fiber

Volume 10, Number 2, April 2018

Hu Liang
Yange Liu
Hongye Li
Hao Zhang
Simeng Han
Yonghua Wu
Zhi Wang

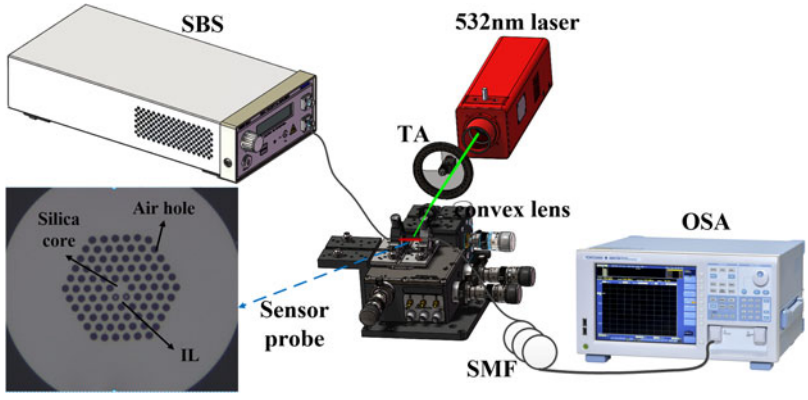

DOI: 10.1109/JPHOT.2018.2822292
1943-0655

All-Fiber Light Intensity Detector Based on an Ionic-Liquid-Adorned Microstructured Optical Fiber

Hu Liang, Yange Liu, Hongye Li, Hao Zhang, Simeng Han, Yonghua Wu, and Zhi Wang

Tianjin Key Laboratory of Optoelectronic Sensor and Sensing Network Technology, Institute of Modern Optics, Nankai University, Tianjin 300071, China

DOI:10.1109/JPHOT.2018.2822292

Manuscript received February 1, 2018; revised March 27, 2018; accepted March 29, 2018. Date of publication April 2, 2018; date of current version April 13, 2018. This work was supported in part by the National Natural Science Foundation of China under Grants 61775107 and 11674177; and in part by the Tianjin Natural Science Foundation China under Grant 16JCZDJC31000. Corresponding author: Zhi Wang (e-mail: zhiwang@nankai.edu.cn).

Abstract: A compact optical fiber light intensity detector based on an ionic-liquid-adorned microstructured optical fiber (MOF) is proposed. The light intensity detector is implemented by splicing an index-guiding MOF with two air holes in the innermost layer infused with ionic liquid (IL) between two segments of single-mode fibers. The transmission spectral characteristics of the proposed intensity detector under different power densities have been investigated from experimental as well as theoretical perspectives. Owing to modal interference effect and intrinsic absorption of the IL, the power density sensitivity reaches 1.5291 dB/(mW•mm^{-2}) within a relatively linear range. The high sensitivity and feasibility of our proposed intensity detector is anticipated to serve as the key element, such as optical switch, in future all-optical networks.

Index Terms: Light intensity detector, ionic liquid, microstructured optical fiber, intermodal interference, intrinsic absorption.

1. Introduction

As an increasingly important sort of functional materials, ionic liquids (ILs) are a new molten salt system that consists of special cation and anion at ambient temperature [1]. Generally speaking, the dipolar interactions play a major role in common molecular liquids. However, the coulomb interaction or hydrogen bonding interactions are dominant in ILs, hence exceptional liquid structures can exist in ILs, which is inconceivable for molecular liquids [2]. Therefore, they demonstrate innovative physicochemical properties like high chemical and thermal stability [3], low melting point [4], high electrical conductivity [5], and high nonlinearity [6]. The blooming studies focus on the applications of ILs as lubricants [7], magnetic functional materials [8], reinforced candidates for processing or dissolving of biomaterials [9], extractive phases in the field of biotechnology [10], etc. Moreover, some ILs present aggregate formation behavior [11], [12] and large nonlinear optical responses under the action of external fields, implying that these functional ILs may find potential applications in the field of microfluidics and photo-electronics. However, the IL-based optical fiber sensors are unexplored up to date.

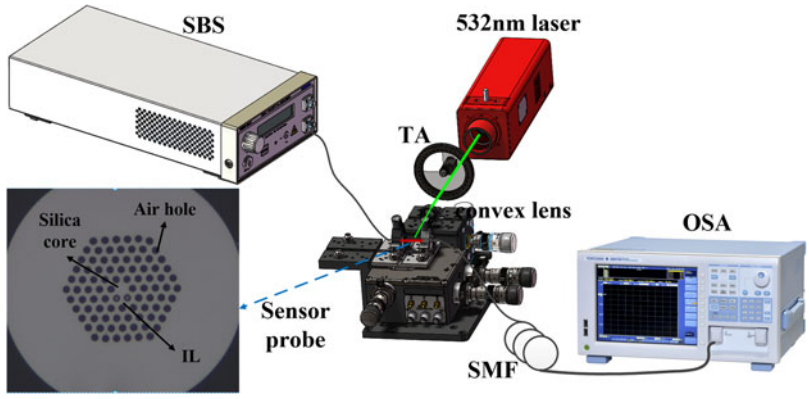

Fig. 1. Schematic diagram of the experimental setup. Inset is the cross sectional image of the IL-adorned MOF.

Due to their significant and promising applications in optical storage, optical modulation, optical switching, and laser manipulation, fiber-based light intensity detectors have been extensively investigated in the advantageous perspectives of portability, immunity to electromagnetic interference, high geometric adaptability, and high sensitivity. A Mach–Zehnder interferometer (MZI) was fabricated by immersing the micro-fiber into ethyl orange solution to measure the light intensity based on wavelength interrogation technique, but it is not simply applicable in real cases for the read out system to detect the peak wavelength shift [13]. A loss-based light intensity detector has been proposed based on the switching effect in an index-matching-liquid-infiltrated photonic bandgap fiber, but the switching effect mainly originates from the thermal effect with laser illumination, making it only suitable for high light intensity detection [14]. Based on the photo-isomerization phenomenon, an intensity-interrogated optical fiber sensor was achieved by azo-photosensitized MOF, but the transmission loss did not exhibit remarkable change and the light intensity variation is concentration dependent [15]. Due to their promising applications in future all-optical networks, it is always valuable to develop novel light-driven fiber-optic devices.

In this letter, a loss-based light intensity detector constituted by an IL-adorned MOF has been proposed and experimentally demonstrated. The detector is implemented by selectively infiltrating two contiguous air holes in the cladding of the MOF with ILs, which leads to multimodal interference between the MOF fundamental core mode and the rod modes supported in the IL-infiltrated air holes. Owing to the modal interference effect of the modified MOF in combination with the absorption properties of the ILs in the near-infrared wave band, light intensity detection with high operability could be achieved based on loss-based interrogation approach.

2. Operation Principle and Experimental Setup

Fig. 1 shows experimental setup for the proposed light intensity detector, which consists of a supercontinuum broadband source (SBS), an optical spectrum analyzer (OSA: operation wavelength ranges from 0.6 μm to 1.7 μm), a sensor probe based on IL-adorned MOF, a 532 nm laser (laser facula area is $\sim 0.5\,\text{mm}^2$), a tunable attenuator (TA) used to adjust the power of the laser, and a convex lens to focus the laser light onto the sensor probe. The sensor probe is fabricated by photosensitizing the MOF with ILs (1-Ethyl-3-methylimidazolium dicyanamide with refractive index (RI) of 1.5307, Moni Chem. Eng. Sci. &Tech. Co., Ltd) based on the direct manual gluing method [16]. The core and cladding diameters of the MOF are 7.4 μm and 125 μm, respectively, and the material refractive index of the background silica is about 1.444 around 1550 nm. Two sections of SMFs are spliced with the modified MOF, and the length of the sensor probe is approximately 1 cm. When the input light is launched into the IL-adorned MOF, both of the fundamental mode and the cladding modes in the IL-infiltrated air-holes could be excited. Due to the overlap and different propagation constants of core mode and cladding modes, modal interference effect occurs

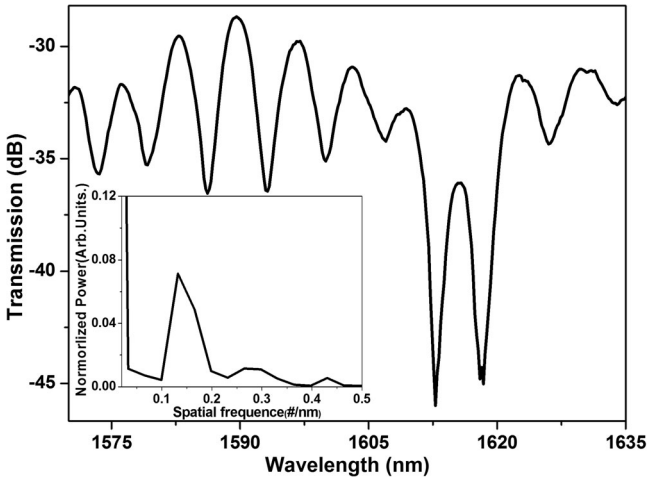

Fig. 2. Transmission spectrum of the proposed device. Inset shows the spatial frequency spectrum.

in the IL-adorned MOF and a fiber-optic Mach-Zehnder interferometer could be achieved [17]. For simplicity, we assume that only two modes contribute to modal interference and the resultant light intensity distribution over the fiber cross section could be described as [18]:

$$I(r, L) = I_0 \left[\eta_1 F_1(r) + \eta_2 F_2(r) + 2(\eta_1 \eta_2)^{1/2} f_1(r) f_2(r) \cos(\Delta\beta L) \right] \tag{1}$$

where η_1 and η_2 are the fractional power of each mode, r is the radial coordinate, $f_1(r)$ and $f_2(r)$ are the radial distributions of the electric field for each mode; $F_1(r) = f_1^2(r)$, $F_2(r) = f_2^2(r)$, L is the length of the sensor probe, namely the length of the IL-adorned MOF, $\Delta\beta$ is the propagation constant difference:

$$\Delta\beta = \frac{2\pi \left(n_{eff1} - n_{eff2} \right)}{\lambda} = \frac{\phi}{L} \tag{2}$$

where n_{eff1} and n_{eff2} respectively refer to the effective RIs, ϕ is the phase difference. According to (2), as an external disturbance (e.g., light intensity in this letter) is applied on the sensor probe, the RI of ILs would change with the disturbance and the effective RI difference would change in the meantime, causing the interference fringe to shift accordingly. The transmission spectrum of the device is shown in Fig. 2. It is clear that the free spectral range (FSR) around 1590 nm is 7.1 nm, and relatively large insertion loss is introduced because of the residual IL at the facet of the MOF during the splicing. It should be noted that two fringe dips abruptly get deepened around 1615 nm. In order to identify the number of the modes participating in the modal interference process, Fourier-transformation is performed onto the transmission spectrum, as shown in the inset of Fig. 2. It is apparent that two spatial frequencies respectively corresponding to the fundamental core mode and one cladding mode are present in the frequency spectrum.

According to two-mode interference principle, we have:

$$FSR = \frac{\lambda^2}{\Delta n_{eff} L} \tag{3}$$

where λ is the wavelength of particular interference dip, Δn_{eff} is the effective RI difference between the two modes [about 3.56×10^{-2} according to (3)]. To confirm what mode takes part in the modal interference process, the effective RI curves of the fundamental core mode and the three primary cladding modes are simulated based on the finite element method (FEM), as shown in Fig. 3, whose insets give the typical mode field distributions. According to calculated values of Δn_{eff}, it could be deduced that the two primary modes participating in modal interference should be the fundamental core mode (d) and the cladding mode (c). Moreover, simulation results show that the effective RI curves of the core fundamental mode and the cladding modes do not intersect in the experimental

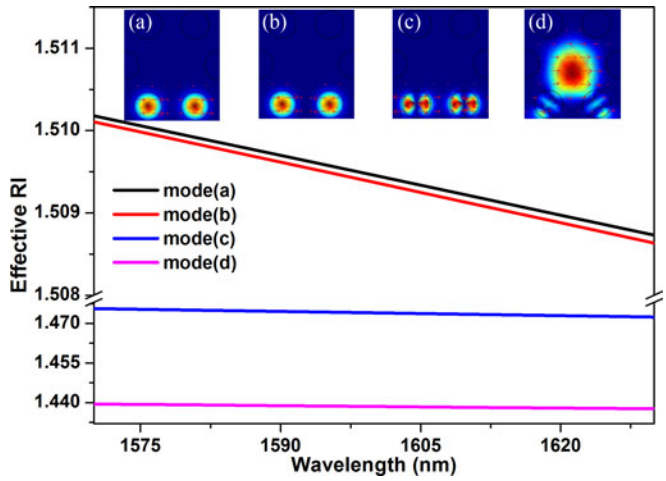

Fig. 3. Dispersion curves of the three primary cladding modes and the core mode. Insets show typical mode field distributions.

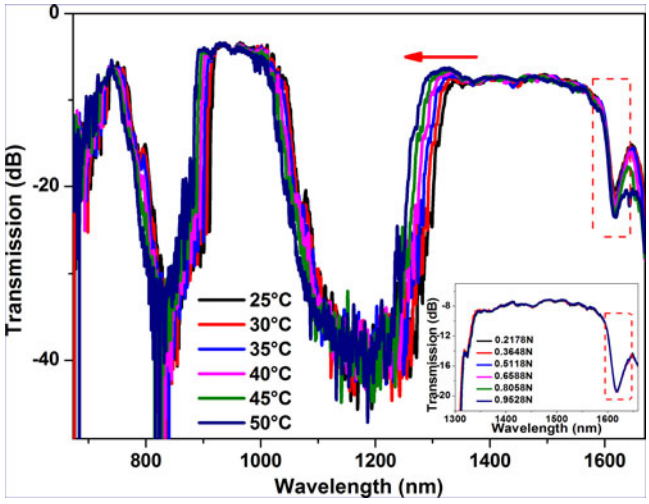

Fig. 4. Transmission spectra of the MOF with all of cladding air holes filled with ILs at different temperatures. Inset is the spectra under different forces.

measurement wavelength range of 1570 nm to 1635 nm, which means that the intermodal phase matching condition could never be satisfied, and in this case the unexpected two fringe dips around 1615 nm cannot result from the resonance coupling effect [19].

To investigate the cause for the deepening of particular interference dips, a MOF with all of the cladding air holes infiltrated with ILs is fabricated to eliminate the influence of intermodal interference. As the RI of the IL is far higher than that of substrate in MOF, photonic bandgap effect is acquired, as shown in Fig. 4. However, a transmission dip appears in one of the bandgaps around 1617 nm, which coincides with the position of the above-mentioned interference dips. The transmission spectral responses to temperature and force have also been investigated, as shown in Fig. 4 and its insets. It could be seen that the bandgap edges show significant shifts, whereas the transmission dip retains its peak wavelength, which indicates that the transmission dip most likely originates from the intrinsic absorption of ILs. Accordingly, the special fringe dips are caused by the resultant action of mode interference effect and the intrinsic absorption of ILs.

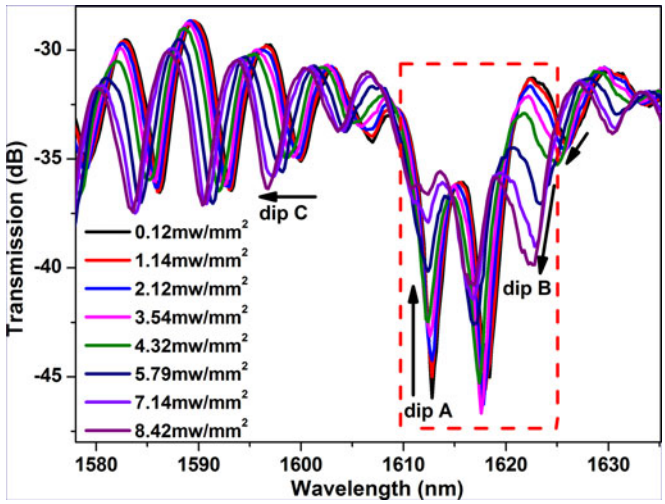

Fig. 5. Transmission spectral evolution under different laser power densities.

3. Experimental Results and Discussion

By rotating the TA to adjust the light intensity, we have studied the transmission characteristics of the proposed detector, as shown in Fig. 5. The transmission spectrum changes considerably in response to the variation of light intensity, and it should be noted that as appropriate laser power level is applied to minimize the light-induced thermal effect, the laser-induced temperature variation is less than 0.4 °C [13]. Dip A, dip B and dip C are selected to investigate the spectral responses of the proposed detector to the variation of laser power density. With the increment of laser power density, all of the interefrence dips (such as dip C) experience significant blueshifts except the ones marked in the red rectangle, whereas the transmission loss of dip A presents dramatic change in comparison to the others, as shown in Fig. 5. For dip B, the transmission loss and dip wavelength both change significantly.

The measurement results for the spectral blueshift could be attributed to the RI change of ILs, which is caused by the possible aggregate formation behavior of the ions under the laser irradiation. Although the ILs have large negative nonlinear RI, to avoid the laser-induced thermal effect, the power density used in our experiment is rather small to excite the nonlinear effect. Moreover, the temperature sensitivity of interference dip wavelength for the proposed MZI could be described as [20]:

$$\frac{d\lambda}{dT} = \frac{\lambda}{\Delta n_{eff}} \left(\frac{dn_{eff1}}{dT} - \frac{dn_{eff2}}{dT} \right) \tag{4}$$

where dn_{eff}/dT is the thermal coefficient of effective refractive index, the calculated temperature sensitivity is approximately 0.893 nm/ °C. Calculation results indicate that the temperature-dependent wavelength shift should be no more than 0.36 nm. Therefore, the ion aggregation may be the dominant factor for the RI change of ILs under the laser irradiation [21]. Generally speaking, the ion aggregation would result in the RI decrease, similar to ferrofluid [22]. Assume the effective RI difference varies from Δn_{eff} to $\Delta n'_{eff}$ due to the RI change of IL induced by ion aggregation, the transmission dip wavelength shift $\Delta\lambda_m$ can be given by [22]:

$$\Delta\lambda_m = \frac{2\left(\Delta n'_{eff} - \Delta n_{eff}\right) L}{2m+1} \tag{5}$$

where m is an integer. Fig. 3 shows that the effective RI for mode (c) is higher than that of the core mode, and when the RI of IL decreases the effective RI difference Δn_{eff} between the core fundamental mode (d) and the cladding mode (c) in the IL-adorned MOF decreases as well, causing

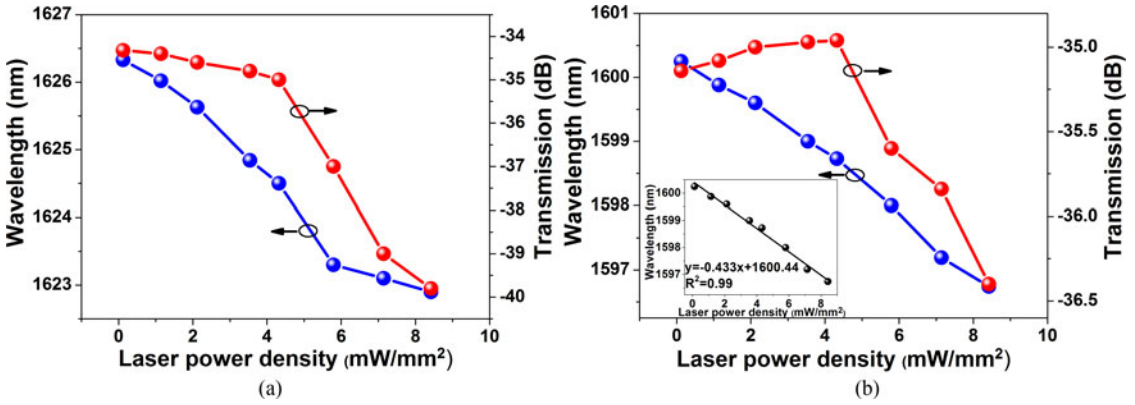

Fig. 6. Transmission loss and wavelength shift as functions of laser power density for (a) dip B and (b) dip C, respectively. Inset shows the linear fitting between wavelength and laser power density for dip C.

a blueshift of the transmission dips according to (5). The experiment results agree well with the above theoretical analysis.

Transmission loss and interference dip wavelength under different laser power densities for dip B are presented in Fig. 6(a). It can be seen that as laser power density increases from 0.12 mW/ mm^2 to 4.32 mW/ mm^2, the transmission loss of dip B increases from -34.35 dB to -35.26 dB, and when the laser power density is further increased to 8.42 mW/ mm^2, the transmission loss increases to -39.89 dB at a faster rate. However, the wavelength shift tends to be faster in the first stage and slower in the second stage, which shows opposite tendency to the transmission loss variation. This phenomenon should be associated with the resultant effects of two-mode interference and the intrinsic absorption of IL. As the laser power density increases from 0.12 mW/ mm^2 to 4.32 mW/ mm^2, modal interference dominantly influences the wavelength shift of transmission dip B, while the transmission loss for this particular transmission dip change slightly. When the laser power density increases to 4.32 mW/ mm^2, dip B shifts to the right edge of the intrinsic absorption dip of ILs, causing dip B to undergo the dramatic increase in transmission loss and the minor change in wavelength. The spectral responses of dip B could reflect the influence of the intrinsic absorption at the interference dip. Since the ion aggregation would change the physical properties of ILs without having impact on its chemical properties, the intrinsic absorption dip of IL would not alter much as laser power density changes. It can be deduced that the dynamic variation of dip B mainly depends on the interference dip wavelength shift and the dramatic increment of transmission loss results from the superposition of absorption dip and fringe pattern. Obviously, dip C derives from modal interference effect and the transmission loss changes irregularly with laser power density. However, the wavelength of dip C varies linearly with a sensitivity of -0.433 nm/(mW $\cdot$ mm^{-2}), as shown in Fig. 6(b).

The relationship between transmission loss and laser power density for dip A is presented in Fig. 7. The transmission spectra exhibit nonlinear responses to the variation of laser power density. And within a power density range of 4.32 mW/mm^2 to 8.42 mW/mm^2, the transmission loss linearly decreases with the increment of the laser power density, and the laser power sensitivity reaches 1.5291 (dB/mW $\cdot$ mm^{-2}) with a R^2 value of 0.9922, as shown in the inset of Fig. 7. It is worthy noted that the wavelength shift of dip A is less than 1 nm during the experimental process, which indicates that such a proposed device is a promising candidate to serve as a loss-based light intensity detector. Since dip A is located on the left edge of the intrinsic absorption dip, wavelength shift of dip A is caused by the minor absorption edge shift and the shift of interference fringes, in no regard to the laser power density. When laser power density decreases, the transmission loss of dip A increases accordingly. The slight deviation of the experimental data from the linear fitting curve should result from the slight temperature variation of ILs under the laser irradiation. As laser power density increases, the number of the aggregated ions would increase accordingly, making

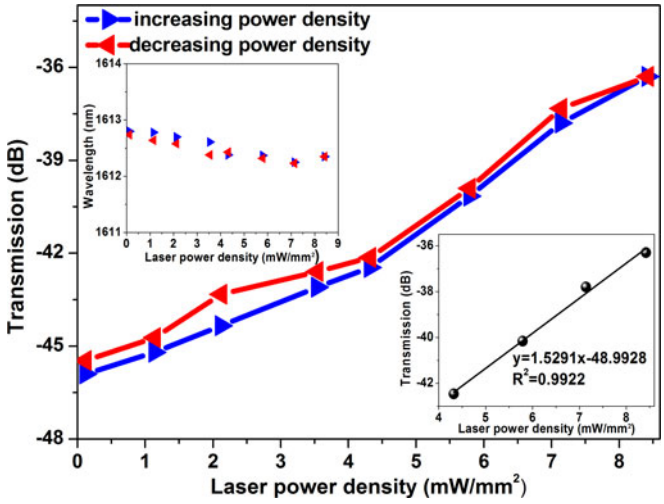

Fig. 7. Transmission loss variation as a function of laser power density for dip A. Insets show the interference dip wavelength versus laser power density and linear fitting between transmission loss and laser power density.

TABLE 1
Comparison of Sensing Performances for the Experimentally Observed Peaks

No.	Wavelength shift (nm)	Transmission variation (dB)	Linear interval (mW/mm^2)	Sensitivity
Dip A	0.55	9.60	4.32~8.42	1.5291 $dB/(mW \cdot mm^{-2})$
Dip B	3.23	5.48	-	-
Dip C	3.51	1.26	0.12~8.42	-0.433 $nm/(mW \cdot mm^{-2})$

them the optical absorption centers. Hence the temperature of the ILs infiltrated in the air holes would slightly increase with the time being.

As summarized in Table 1, light intensity detection with wider measurement range could be achieved based on the wavelength-interrogation approach using dip C. However, in order to reduce the complexity of sensing demodulation, the proposed device could also be employed as a detector based on intensity interrogation using dip A. Moreover, the detector has such merits as ease of fabrication, good reliability and high sensitivity, which ensure its applicability for practical uses.

4. Conclusion

In conclusion, a loss-based light intensity detector based on an IL-adorned MOF has been proposed and experimentally demonstrated by infiltrating ILs into two air holes to construct a modal interferometer. The RI changes of the ILs induced by laser irradiation would lead to the interference dip wavelength shift. Owing to the resultant effects of modal interference and the intrinsic absorption of ILs, the power density sensitivity reaches 1.5291 $dB/(mW \cdot mm^{-2})$ as the laser power density increases from 4.32 mW/mm^2 to 8.42 mW/mm^2. Owing to its desirable merits such as high sensitivity, low cost, compact size and high feasibility, the proposed IL-based optical fiber sensor provides a promising candidate for light intensity detection. And moreover, such a detector paves a new way toward developing light-driven fiber-optic devices by combining the optical fiber transmission properties with material characteristics of ILs for future all-optical networks.

References

[1] T. Welton, "Room-temperature ionic liquids. solvents for synthesis and catalysis," *Chem. Rev.*, vol. 99, no. 8, pp. 2071–2083, Apr. 1999.

[2] S. Hayashi, S. Saha, and H. Hamaguchi, "A new class of magnetic fluids: Bmim[$FeCl_4$] and nbmim[FeCl4] ionic liquids," *IEEE Trans. Magn.*, vol. 42, no. 1, pp. 12–14, Jan. 2006.

[3] M. Tariq, P. A. S. Forte, M. F. C. Gomes, J. N. C. Lopes, and L. P. N. Rebelo, "Densities and refractive indices of imidazolium- and phosphonium-based ionic liquids: Effect of temperature, alkyl chain length, and anion," *J. Chem. Thermodyn.*, vol. 41, no. 6, pp. 790–798, Jan. 2009.

[4] A. N. Soriano, B. T. D. Jr, and M. H. Li, "Measurements of the density and refractive index for 1-n-butyl-3-methylimidazolium-based ionic liquids," *J. Chem. Thermodyn.*, vol. 41, no. 3, pp. 301–307, Aug. 2009.

[5] N. V. Likhanova, M. A. D. Aguilar, O. O. Xometl, N. N. Entzana, E. Arce, and H. Dorantes, "The effect of ionic liquids with imidazolium and pyridinium cations on the corrosion inhibition of mild steel in acidic environment," *Corros. Sci.*, vol. 52, no. 6, pp. 2088–2097, Feb. 2010.

[6] R. F. Souza, M. A. R. C. Alencar, M. R. Meneghetti, J. Dupont, and J. M. Hickmann, "Nonlocal optical nonlinearity of ionic liquids," *J. Phys., Condens. Matter*, vol. 20, no. 15, pp. 785–790, Mar. 2008.

[7] F. Zhou, Y. Liang, and W. Liu, "Ionic liquid lubricants: Designed chemistry for engineering applications," *Chem. Soc. Rev.*, vol. 38, no. 9, pp. 2590–2599, Jun. 2009.

[8] M. Okuno and H. Hamaguchi, "Magnetic manipulation of materials in a magnetic ionic liquid," *Appl. Phys. Lett.*, vol. 89, no. 13, Sep. 2006, Art. no. 132506.

[9] M. G. Freire, A. R. R. Teles, R. A. S. Ferreira, L. D. Carlos, J. A. L. Silva, and J. A. P. Coutinho, "Electrospun nanosized cellulose fibers using ionic liquids at room temperature," *Green Chem.*, vol. 13, no. 11, pp. 3173–3180, Aug. 2011.

[10] S. P. M. Ventura, S. G. Sousa, M. G. Freire, L. S. Serafim, A. S. Lima, and J. A. P. Coutinho, "Design of ionic liquids for lipase purification," *J. Chromatogr. B.*, vol. 879, no. 26, pp. 2679–2687, Jul. 2011.

[11] S. Dorbritz, W. Ruth, and U. Kragl, "Investigation on aggregate formation of ionic liquids," *Adv. Synth.Catal.*, vol. 347, no. 9, pp. 1273–1279, Mar. 2005.

[12] A. G. Saiz *et al.*, "A magnetic ionic liquid based on tetrachloroferrate exhibits three-dimensional magnetic ordering: A combined experimental and theoretical study of the magnetic interaction mechanism," *Chem. Eur. J.*, vol. 20, no. 1, pp. 72–76, Dec. 2013.

[13] H. Liu *et al.*, "A light-intensity-controlled microfiber-assisted Mach–Zehnder interferometer based on ethyl orange solution under 532 nm laser excitation," *Sens. Actuators. B, Chem.*, vol. 216, pp. 229–234, Apr. 2015.

[14] J. Guo *et al.*, "Broadband optically controlled switching effect in a microfluid-filled photonic bandgap fiber," *J. Opt.*, vol. 18, no. 5, Feb. 2016, Art. no. 055706.

[15] C. Yang *et al.*, "Light intensity sensor based on an Azo-infiltrated microstructured optical fiber," *IEEE Photon. Technol. Lett.*, vol. 26, no. 24, pp. 2458–2461, Dec. 2014.

[16] B. T. Kuhlmey, B. J. Eggleton, and D. K. C. Wu, "Fluid-filled solid-core photonic bandgap fibers," *J. Lightw. Technol.*, vol. 27, no. 11, pp. 1617–1630, Jun. 2009.

[17] H. Liang *et al.*, "Fiber in-line Mach–Zehnder interferometer based on near-elliptical core photonic crystal fiber for temperature and strain sensing," *Opt. Lett.*, vol. 38, no. 20, pp. 4019–4022, Oct. 2013.

[18] W. J. Bock, T. A. Eftimov, P. Mikulic, and J. H. Chen, "An inline core-cladding intermodal interferometer using a photonic crystal fiber," *J. Lightw. Technol.*, vol. 27, no. 17, pp. 3933–3939, Sep. 2009.

[19] C. P. Lin *et al.*, "Liquid modified photonic crystal fiber for simultaneous temperature and strain measurement," *Photon. Res.*, vol. 5, no. 2, pp. 129–133, Apr. 2017.

[20] M. Yang, D. N. Wang, Y. Wang, and C. R. Liao, "Fiber in-line Mach–Zehnder interferometer constructed by selective infiltration of two air holes in photonic crystal fiber," *Opt. Lett.*, vol. 36, no. 5, pp. 636–638, Mar. 2011.

[21] T. Akitsu and Y. Einaga, "Novel photo-induced aggregation behavior of a supramolecular system containing iron(III) magnetic ionic liquid and azobenzene," *Inorg. Chem. Commun.*, vol. 9, no. 11, pp. 1108–1110, Jul. 2006.

[22] M. Deng, C. Huang, D. H. Liu, W. Jin, and T. Zhu, "All fiber magnetic field sensor with Ferrofluid-filled tapered microstructured optical fiber interferometer," *Opt. Exp.*, vol. 23, no. 16, pp. 20668–20674, Jul. 2015.